JOURNAL OF Materials CHEMISTRY

New molecular and supermolecular polymer architectures *via* transition metal catalyzed alkene polymerization†

Jürgen Suhm,[a] Johannes Heinemann,[a] Yi Thomann,[a] Ralf Thomann,[a] Ralph-Dieter Maier,[a] Thomas Schleis,[b] Jun Okuda,[b] Jörg Kressler[b] and Rolf Mülhaupt*[b]

[a]*Freiburger Materialforschungszentrum und Institut für Makromolekulare Chemie der Albert-Ludwigs Universität, Stefan-Meier-Str. 21, D-79104 Freiburg i.Br., Germany*

[b]*Institut für Anorganische und Analytische Chemie, Johannes Gutenberg Universität, Mainz, Joh.-Joachim-Becher Weg 24, D-55099 Mainz, Germany*

Superstructure formation during crystallization has been examined as a function of isotactic poly(propene) and poly(ethene) molecular architectures, tailored by means of metallocene catalyzed propene polymerization, metallocene catalyzed ethene/alk-1-ene copolymerization, and nickel-catalyzed migratory insertion polymerization of ethene to afford methyl-branched poly(ethene) without using comonomers. The role of steric irregularities in the chain resulting from false insertion in stereoselective polymerization or from short chain branching, respectively, was investigated. Randomly distributed regio- and stereo-regularities in isotactic poly(propene) chains and variation of crystallization temperature were the key to controlled poly(propene) crystallization and predominant formation of the γ-modification. Poly(propene) melting temperature increased with increasing isotactic segment length between stereo- and regio-irregularities. Superstructures of isotactic γ-poly(propene) were analyzed by means of light and atomic force microscopy. Both types of short-chain branched poly(ethene)s, prepared by ethene/oct-1-ene copolymerization and migratory insertion homopolymerization, showed similar dependence of melting temperature on the degree of branching, calculated as the number of branching carbon atoms per 1000 carbon atoms. Phase transitions were monitored by means of wide angle X-ray scattering and pressure–volume–temperature measurements. Atomic force microscopy was applied to image both lamella- and fringed micelle-type superstructures as a function of the degree of branching.

Introduction

In nature highly active and stereoselective enzyme catalysts polymerize twenty aminoacids to produce sophisticated proteins with very well defined molecular mass and accurately controlled comonomer sequence. Excellent control of molecular architecture, predetermined by the genetic code, is the prime requirement to produce functional protein superstructures with tailor-made properties *via* self-assembly of individual polypeptide chains. In contrast, most industrial catalyst systems useful in alkene and styrene polymerization give rather ill defined polymers, as reflected by fairly broad distributions of their molecular masses and comonomer sequences. However, with respect to the early catalyst generations introduced during the 1950s following the pioneering advances of Ziegler and Natta, remarkable progress has been made during the last decade. Modern transition metal catalysts applied in ethene and propene homo- and co-polymerization reach bench marks set by catalyst productivities and turnover typical for enzyme catalysts. Catalyst residues, being equivalent to <1 ppm transition metal, can be left in the polymer, thus eliminating catalyst deactivation and removal of transition metal compounds from the polyalkenes. Stereoselectivity with respect to formation of high molecular mass isotactic poly(propene) (i-PP) has been improved to $>99\%$, thus eliminating the need for extensive purification of byproducts, *e.g.*, low molecular mass fractions and tacky atactic poly(propene)s, by means of solvent extraction. During the early 1960s up to 200 kg landfill per 1000 kg i-PP was obtained as byproducts of poly(propene) production, whereas today modern gas phase processes represent prime examples for environmentally friendly processes without solvent emission and essentially complete conversion without byproduct formation. Progress in poly(propene) catalyst, process, and application technology was compiled in a multi-author handbook edited by Moore.[1] As a commodity polymer, poly(propene) combines low price with high heat distortion temperatures, low mass, corrosion resistance, wide range of properties and applications, ranging from automotive injection molding parts to baby diapers. Moreover, modern polyalkenes are very compatible with recycling strategies such as remolding, feedstocks and energy recovery. Owing to the low energy demand during catalytic low pressure polymerization, polyalkenes retain oil-like high energy content. In fact, poly(propene) and other polyalkenes represent a solid high molecular mass modification of oil with very similar hydrocarbon structure. After completing their product life cycles, polyalkenes are readily converted back into liquid oil and gas upon heating above 400 °C. Therefore, it is not suprising that poly(propene) exhibits higher growth rates with respect to other commodity plastics and is competing very successfully with other materials, including engineering plastics, and also less ecologically and economically attractive polymers. Soon poly(propene) production is expected to surpass that of PVC in Western Europe.

During the last decade, new catalyst systems have been developed which simplify polyalkene production processes and offer very attractive opportunities of preparing tailor-made polyalkenes in very high yields and of improving better understanding of correlations between catalyst structures, polymer microstructures, polymer properties and polymer processing. Prominent examples of innovative chemistry represent the development of metallocene catalysts. Prospects and mechanisms of metallocene catalyzed alkene polymerization were reviewed by Brintzinger *et al.*,[2] Kaminsky,[3] and Hamielec and Soares.[4] In contrast to most conventional catalyst systems, industrial metallocene catalysis—introduced during the mid 1980s—offers several advantages. Metallocene catalysts are composed of essentially a single type of catalytically active center, which produces very uniform homo- and co-polymers

† Presented at the Third International Conference on Materials Chemistry, MC[3], University of Exeter, Exeter, 21–25 July 1997.

with narrow molecular mass distributions, reflected by polydispersities of $M_w/M_n \approx 2$, and molecular mass independent uniform comonomer incorporation, covering the entire composition range feasible for ethene/alk-1-ene copolymers. Metallocene-based polyalkenes give much less extractable fractions with respect to conventional polyalkenes, which frequently represented complex mixtures of polymer chains having different molecular mass and comonomer content. Furthermore, metallocene catalysis gives excellent control of molecular mass, end groups and polyalkene molecular architectures such as stereochemistry as well as short- and long-chain branching. The industrially very attractive novel families of metallocene-based copolymers include ethene copolymers with high content of alk-1-ene comonomer, *e.g.*, oct-1-ene, and long-chain branched poly(ethene)s, and ethene copolymers ranging from linear low density poly(ethene) to ultra low density poly(ethene) with densities of 0.88 to 0.92 g cm^{-3} (LLDPE), thermoplastic elastomers (plastomers), ethene/propene/diene rubber (EPDM), and impact-modified poly(propene) including various reactor blends. Since 1988 syndiotactic poly(propene)[5] has also become available on an industrial scale. In earlier days, syndiotactic poly(propene) was an example of a typical exotic laboratory chemical, produced in poor stereoselectivities at $-78\,^{\circ}C$ with productivities of 1 g polymer (g transition metal)$^{-1}$ within 24 h. Today most metallocene catalysts produce poly(propene) of various stereoregularities in yields exceeding 1 metric tonne (g transition metal)$^{-1}$ within an hour. Large amounts of by-products in conventional polymer required reevaluation of crystallization behavior when modern syndiotactic poly(propene) became available. Crystallization of iso- and syndiotactic poly(propene) including metallocene-based poly(propene) and visualization by means of atomic force microscopy was reviewed by Lotz, Wittmann and Lovinger.[6]

In addition to highly stereoregular poly(propene)s high molecular mass stereoblock and segmented low stereoregular poly(propene) also became available as thermoplastic elastomers and blend components. Stereoblock poly(propene), consisting of alternating isotactic and low stereoregular segments, was obtained with special metallocene catalysts such as methylaluminoxane (MAO)-activated HMeC(Ind)(Me_4Cp)$TiCl_2$, reported by Chien and co-workers,[7] and MAO-activated (2-Ph-Ind)$_2ZrCl_2$, reported by Coates and Waymouth.[8] Transmetallation with aluminium alkyls was applied by Chien *et al.*[9] to transfer poly(propene) between different catalytically active sites during chain propagation in order to produce stereoblock polymers such as syndiotactic poly(propene)-*block*-isotactic poly(propene). For the first time, high molecular mass atactic poly(propene) is now available using (Flu)$_2ZrCl_2$/MAO as reported by Resconi *et al.*[10,11]

In addition to poly(alk-1-ene)s with controlled stereochemistry a large number of copolymers were also produced by means of metallocene catalysis. In contrast to conventional Ti-based catalyst, half-sandwich metallocene-based catalysts produce styrene co- and ter-polymers with ethene without encountering polystyrene byproduct formation.[12–14] Vinyl end groups of poly(ethene) are copolymerized to afford long-chain-branched poly(ethene) and ethene/oct-1-ene copolymers which exhibit much better processing properties due to shear thinning of the resulting poly(ethene) melts.[15] Novel families of ethene/cycloalkene copolymers, *e.g.*, ethene/norbornene, expand the range of polyalkene materials in the field of amorphous, optically transparent materials with high glass transition temperature and low water-uptake for applications as optical data storage media and medical packaging.[16,17] In an alternative process for production of cycloaliphatic copolymers, ethene polymers containing cyclopentane units in the backbone were prepared by means of cyclocopolymerization of hexa-1,5-diene and ethene.[18]

During the mid 1980s, Fink *et al.*[19–21] reported an intriguing new synthesis for branched poly(ethene) without using comonomer by means of nickel-catalyzed alkene polymerization. In his so-called '2,ω-polymerization', pent-1-ene did not form poly(pent-1-ene) according to 1–2 insertion of pent-1-ene as expected for conventional catalysts. Instead, Fink obtained methyl-branched poly(ethene), which is equivalent to the alternating ethene/propene copolymer in the case of pent-1-ene polymerization. Higher alk-1-enes gave methyl-branched polyethene where the distance between methyl branches is controlled *via* the length of the alk-1-ene. This rather peculiar behaviour was attributed by Fink to migratory insertion, where the transition alkyl migrates along the polymer chain *via* repeated β-hydride transfer and reinsertion into the resulting alkene unsaturated polyethene chain. This methyl-branching due to migratory insertion, also referred to as 'chain walking' was observed by Brookhart and others[22] for ethene polymerization with MAO-activated nickel bisimine and palladium bisimine alkyl/borate complexes. In contrast to many titanium based systems, Brookhart's palladium bisimine catalysts tolerate polar comonomers. In the presence of alkyl acrylates, the simultaneous insertion and migration combined with ethene/alkylacrylate copolymerization accounts for formation of poly(ethene) with pendent alkyl and ester-terminated alkyl substituents.[23]

This remarkable progress, achieved during the 1990s in alkene polymerization, offers attractive potential to modify the molecular architectures of poly(propene)s as well as branched poly(ethene)s without byproduct formation and sacrificing narrow molecular mass distributions. Polyalkenes represent 'finger prints' of the catalytically active transition metal alkyl compounds, which can be designed to tailor polyalkene architectures. The objective of this research was to exploit metallocene based propene homopolymerization and controlled formation of short-chain branched poly(ethene) *via* metallocene-catalyzed ethene copolymerization with oct-1-ene and *via* migratory insertion ethene homopolymerization to produce well defined model polyalkenes, containing randomly distributed steric irregularities in the polyalkene backbone. Owing to the random interruption of crystallizable polymer backbones, it was expected to influence morphology development during crystallization. In the case of poly(propene) such steric irregularities reflect false insertions. In the case of poly(ethene) steric irregularities result from random incorporation of oct-1-ene comonomer or methyl- and alkyl-branching due to migratory insertion during ethene homopolymerization. The role of such irregularities, more specifically the segment length of the polymer chain in between two steric irregularities, was investigated for crystallization of isotactic poly(propene) and short-chain branched poly(ethene). Atomic force microscopy was applied to visualize superstructure formation during crystallization.

Experimental

Polymerization

The polymerization procedure of the propene polymers has been described previously by the groups of Jüngling and Fischer,[24,25] the copolymerization procedure of ethene and oct-1-ene and the properties of the respective polymers are given by Schneider *et al.*[26,27] The synthesis and investigations on ethene/oct-1-ene copolymers using commercially available EO 02, referring to 2 mass% oct-1-ene incorporation, and EO25, referring to 25 mass% oct-1-ene incorporation (Engage™ and Affinity™) made by Constrained Geometry Catalysts (CGC) and EO 38, referring to 38 mass% oct-1-ene incorporation, and EO55 referring to 55 mass% oct-1-ene incorporation made by *rac*-dimethylsilylenebis(2-methylbenz[e]indenyl)-zirconium dichloride (MBI) catalysis are reported elsewhere.[28] The ethene polymerization reactions using dibromo-[glyoxalbis(2,6-diisopropylphenylimine)]nickel (DHN) and dibromo-[2,6-diacetylbis(2,6-diisopropylphenylimine)]nickel (DMN) catalysts were performed in a 1 l mechanically stirred

glass reactor. Typically, 400 ml toluene were pumped into the glass reactor. After thermal equilibration of the reactor system ethene was continously added by a mass-flow meter (F-111C, Bronkhorst, Nl-7261 AK Ruurlo, Netherlands) until the reaction mixture was saturated with ethene. The polymerization was started by adding 8 μmol of DHN or DMN in a 10 ml 1 : 1 mixture of toluene and MAO solution, respectively, equivalent to $[Ni] = 20\ \mu mol\ l^{-1}$ and $[Al] = 20\ mmol\ l^{-1}$. The degree of branching was investigated as a function of catalyst structure (DHN or DMN), polymerization temperature and ethene concentration, respectively. The vapour pressure of the solvent was considered when calculating the ethene concentration. Typically, after 1 h polymerization was quenched by adding 10 ml propan-2-ol. The polymer was precipitated in 1.5 l methanol acidified with 10 ml 10 mass% aq. HCl, filtered and dried at 60 °C under vacuum.

^1H NMR spectra were recorded from solutions of 40 mg of polymer in 0.5 ml $C_2D_2Cl_4$ at 400 K by a Bruker ARX 300 at 300 MHz; ^{13}C NMR spectra at 75.4 MHz, with a 30° pulse angle, 5 s delay and at least 8000 scans. The signals were referenced to $C_2D_2Cl_4$ ($\delta = 74.06$). Melting temperatures, T_m, and glass temperatures, T_g, were determined by means of differential scanning calorimetry (DSC) with a Perkin Elmer Series 7 from the heating curve at a heating rate of 20 K min^{-1}.

Atomic force microscopy

The samples used to study the crystalline morphology by AFM were prepared by melting the powder of the as-prepared and dried polymer between two cover glasses. The samples were held for 10 min at 180 °C and then cooled to room temperature at a rate of 0.2 °C min^{-1}. The prepared films were etched to remove amorphous material from the surface. The etching reagent was prepared by stirring 0.02 g potassium permanganate in a mixture of 4 ml sulfuric acid (95–97%) and 10 g orthophosphoric acid. The *ca.* 5 mm thick films were immersed into the fresh etching reagent at room temperature and held there for 1 h. Initially the samples were held in an ultrasonic bath for 30 min. For subsequent washings, a mixture of two parts by volume of concentrated sulfuric acid and seven parts of water was prepared and cooled to near its freezing point with dry-ice in propan-2-ol. The samples were washed successively with 30% aqueous hydrogen peroxide in order to remove any manganese dioxide present. The samples were washed with distilled water. Each washing was aided with an ultrasonic bath. The AFM experiments were carried out with a 'Nanoscope III' scanning probe microscope (Digital Instruments) at ambient conditions in the tapping mode/phase imaging.

Wide angle X-ray scattering (WAXS) measurements

WAXS measurements were carried out with a Siemens D500 apparatus. For the measurements the Cu-Kα radiation of wavelength $\lambda = 0.154$ nm was used. The samples were held for 10 min at 180 °C and then cooled to room temperature at 0.2 K min^{-1}.

Pressure–volume–temperature (PVT) measurements

Polymer densities were measured at 25 °C and atmospheric pressure using a Micropycnometer (Quantachrome). The changes in density as a function of temperature and pressure were determined with a Gnomix PVT Apparatus (Boulder, CO, USA).[29] The sample cell contained *ca.* 1 g of polymer and mercury as a confining fluid. The measurements were performed in the isothermal mode, *i.e.* the sample was held at a certain temperature and the pressure was continuously raised from 10 to 200 MPa with pressure, volume and temperature being recorded in steps of 10 MPa. The specific volume corresponding to atmospheric pressure was extrapolated by the Tait equation using the PVT software. Subsequently, this procedure was repeated for other temperatures between 30 and 270 °C.

Results and Discussion

Crystallization behavior of isotactic poly(propene) containing randomly distributed stereo- and regio-irregularities

Since the pioneering days of Ziegler–Natta catalysis, the major thrust of catalyst development in propene polymerization was aimed almost exclusively at improving simultaneously both catalyst productivities, reflected by low content of residual transition metal in the polymer, and high stereoselectivity with respect to exclusive formation of highly stereoregular poly(propene), reflected by low content of extractable low stereoregular fraction. As pointed out recently by Randall,[30] despite very high stereoselectivities, poly(propene) macromolecules are seldom 100% isotactic, but possess long isotactic sequences interrupted by stereo- and regio-irregularities. However, many conventional supported Ti-based catalysts give mixtures of highly isotactic, high molecular mass poly(propene) with low stereoregular poly(propene)s exhibiting much lower molecular mass. This is a result of the presence of multiple catalytically active sites, which exhibit different stereoselectivities and ratios of chain propagation rate to chain termination rate, as reflected by the degree of polymerization. In the past, solvent fractionation was applied to separate such rather ill defined poly(propene) samples into better defined fractions.

The prime advantage of metallocenes, often referred to as single site catalysts, is the presence of exclusively one type of catalytically active site. This means that variation of catalyst structure gives control of stereoselectivity and translates into controlled variation of the content of steric irregularities in the poly(propene) backbone without producing mixtures of different polymers produced at different sites. As a consequence, metallocene catalysts can be designed to tailor poly(propene) molecular architectures. This has been demonstrated impressively in the case of metallocene-based propene polymerization. Today it is well accepted that stereoselectivity as well as regioselectivity depend upon the metallocene structure. As reviewed by Brintzinger *et al.*[2] the symmetry of the catalytically active 14 π-electron cationic metallocene alkyl appears to be the key to stereoselectivity. While C_s symmetrical metallocenes produces syndiotactic PP, the C_2 symmetrical metallocenes are known as components of isoselective catalysts. Recently, Fink and co-workers[31] developed a more universal model, which describes the polyalkene microstructures, by considering the lowest energy conformers of the metallocene species coordinating to the prochiral propene monomer, and taking into account the positional changes that polymer chains undergo during polymerization. Fig. 1 illustrates the influence of metallocene structure on polymer properties. The metallocene ligand substitution pattern is also important to prevent chain transfer to monomer. When 2-methyl substituents are introduced in the 2-position of a bisindenyl, chain transfer to monomer is prevented and propene monomer is involved exclusively in chain propagation. This gives much higher molecular masses, which increase with increasing propene pressure. Moreover, benzannelation appears to promote higher catalyst activity, most likely by suppressing reversible catalyst deactivation, *e.g.*, *via* formation of binuclear cationic zirconocene complexes. The influence of 2-methyl substitution and benzannelation was reported by Jüngling *et al.*[32]

The steric irregularities in propene homopolymerization result from false insertions. When '2–1' insertion occurs during repeated '1–2' insertion regioirregular $CH_2CH(CH_3)CH(CH_3)CH_2$ ('head-to-head') units can be detected by means of ^{13}C NMR spectroscopy in the isotactic poly(propene) backbone.[33] When '2–1' insertion takes place, the resulting secondary alkyls are less reactive in alkene

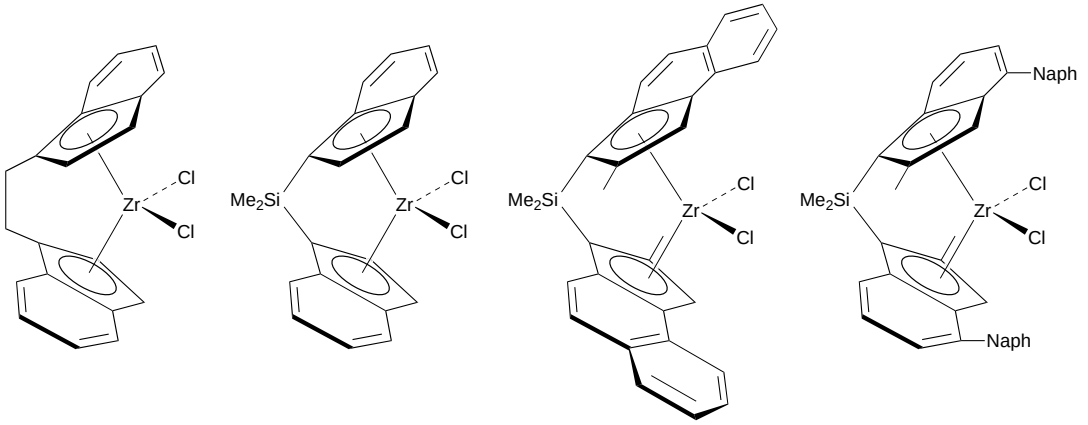

M_w:	24000	36000	330000	875000
(*mmmm*) (%):	78.5	81.7	88.7	99.1
T_m/°C:	132	137	146	161

Fig. 1 Isoselective propene polymerization using MAO activated *rac*-Et(Ind)$_2$ZrCl$_2$ (abbreviated EtI), *rac*-Me$_2$Si(Ind)$_2$ZrCl$_2$ (I), *rac*-Me$_2$Si(2-Me-Benz-Ind)$_2$ZrCl$_2$ (MBI) and *rac*-Me$_2$Si(4-naphthyl-Ind)$_2$ZrCl$_2$ for isoselective propene polymerization (data taken from Spaleck and co-workers[37])

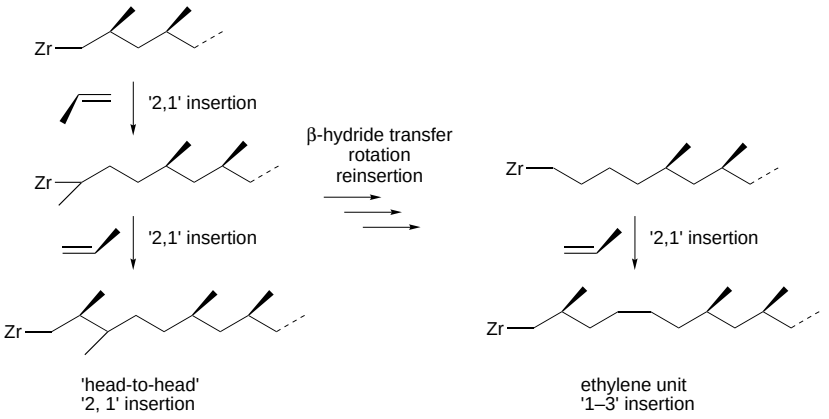

Fig. 2 Formation of regioirregularities during propene polymerization

insertion but can undergo β-hydride transfer to form an alkene-terminated poly(propene) chain. In competition with this chain termination process, reinsertion according to '1–2' type insertion can occur after rotation, which forms the sterically less hindered and hence more reactive alkene-terminated poly(propene). This reinsertion yields poly(propene) which contains isolated ethene units, corresponding to the so-called '1–3' insertion.[34] Interestingly, '1–3' insertion results in formation of propene/ethene copolymers without using ethene as a comonomer. False insertion of propene, *i.e.*, attack of the wrong enantioface of the prochiral propene monomer, produces stereoirregularities, reflected by the *mrrm* pentad sequence typical for steric control by the chirality of catalytically active sites, or *mrmm* pentad sequence typical for chain end control, where the configuration of the last propene unit decides which enantioface is preferably attacked prior to insertion into the metal alkyl bond. The mechanisms responsible for formation of regioirregularities are displayed in Fig. 2.

As a function of metallocene architecture it is possible to incorporate random steric irregularities into the isotactic poly(propene) backbone (*cf*. Fig. 3). The isotactic segment length in between two steric irregularities (n_{iso}), can be calculated according to eqn. (1), which was first proposed by Fischer and Mülhaupt.[35]

$$n_{iso} = P_n/[1 + P_n(W_{mrrm} + W_{2,1})] \quad (1)$$

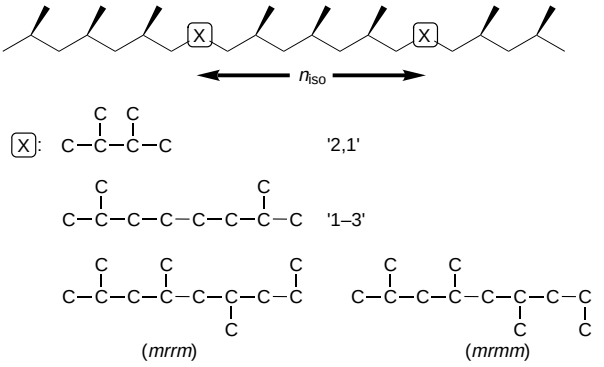

Fig. 3 Stereo- and regio-irregularities are randomly placed along the poly(propene) chain

where P_n is the degree of polymerization, W_{mrrm}, $W_{2,1}$ are the probabilities of the occurrence of stereo- or regio-irregularities, respectively. When data from Fischer and propene homopolymerizations, reported by Jüngling[36] for various catalysts of the silylene bridged bisindenyl ligand framework family, there exists a clear correlation between the average isotactic segment length and the melting temperature of poly(propene)s. As a function of the isotactic segment length the melting

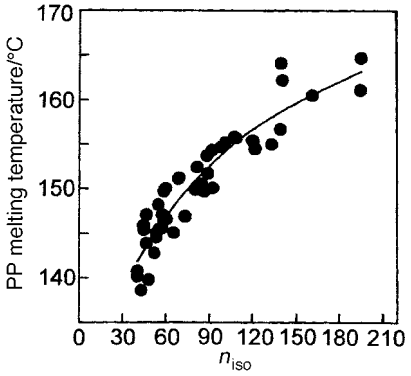

Fig. 4 Correlation between isotactic segment length (n_{iso}) and poly(propene) melting temperature

temperature varies from 130 to 161 °C (Fig. 4). Lower melting poly(propene)s are attractive with respect to their improved heat sealability in packaging applications. In accord with observations by Spaleck *et al.*,[37] typical features of metallocene-based poly(propene)s are low content of extractable fraction, higher stiffness and improved optical clarity.

Furthermore, it is interesting to study the formation of different isotactic poly(propene) modifications as a function of chain architecture. The polymorphism of poly(propene) is still an interesting and not completely understood phenomenon even though it has attracted a lot of research since the early work of Natta. Isotactic polypropene forms exclusively a 3_1 helix and crystallizes in three different modifications.[6] The α modification was already determined by Natta and Corradini.[38] The monoclinic unit cell has the parameters $a=$ 6.65 Å, $b=20.96$ Å, $c=6.5$ Å, $\beta=99.80°$. The β modification crystallizes into a trigonal unit cell with the parameters $a=$ $b=11.01$ Å, $c=6.5$ Å. It forms a frustrated lattice because the helices have a different surrounding and they are not equivalent which is prohibited in classical polymer crystallography.[39] A unique example for non-parallel chain packing into the crystal of a synthetic polymer is the γ modification of isotactic polypropene.[40] It forms an orthorhombic unit cell ($a=8.54$ Å, $b=9.93$ Å, $c=42.41$ Å) composed of bilayers of two parallel helices as shown in Fig. 5.

The direction of the chain axis in adjacent bilayers is tilted with an angle of 80°. This behaviour is very similar to the well known cross-hatching of i-PP in the α modification.[41] In this case daughter lamellae can grow onto existing lamellae in a homoepitaxial manner as in an angle of 80°, respectively. The predominant supermolecular appearance of the α modification is as spherulites.[42] In contrast the γ phase of i-PP forms different morphologies observed by polarized light microscopy as displayed in Fig. 6.

Elongated bundle-like morphologies can be observed.[43] This sample was isothermally crystallized at 110 °C and WAXS measurments show hardly any content of the α modification. The formation of the γ phase is closely related to the microstructure of isotactic poly(propene). The sample shown in Fig. 6 has low stereoregularity. It contains 81.5% *mmmm*, 8.8% *mmmr*, 0.1 *rmmr*, 6.5% *mmrr*, 0.2% *rrrm* and 2.9% *mrrm* pentads. Furthermore, this sample has an M_w of only 18 000 g mol^{-1} and M_w/M_n is 1.6. The average isotactic segment length, n_{iso}, responsible for the formation of the γ phase is 22.4 monomer units. Fig. 7 shows the maximum γ-content of high molecular mass isotactic poly(propene), isothermally crystallized, as a function of the average isotactic sequence length, n_{iso}. Generally, the γ-content increases with increasing crystallization temperature. In the n_{iso} range studied, it is obvious that the γ-content increases with decreasing n_{iso} in the isotactic poly(propene).

In conclusion, the formation of the γ modification can be promoted *via* steric irregularities and specific features of individ-

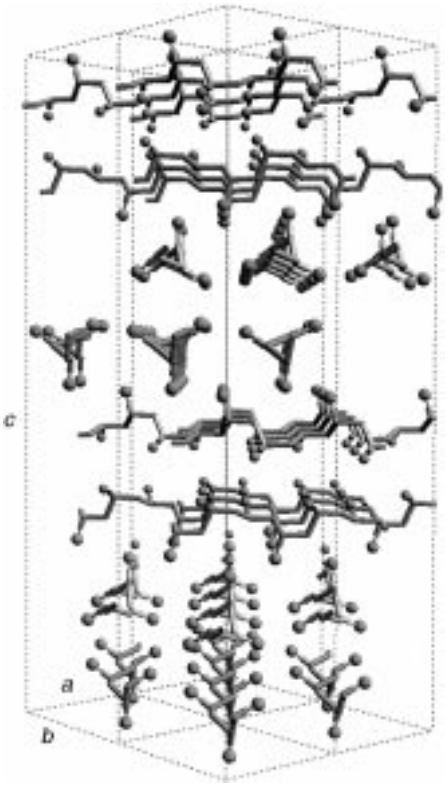

Fig. 5 Schematic drawing of the packing of isotactic poly(propene) helices into four unit cells in the γ-modification

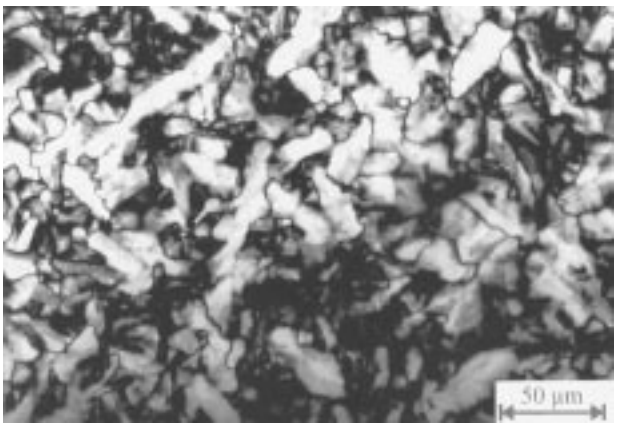

Fig. 6 Polarized light micrograph of an isotactic poly(propene) with >95% γ-modification

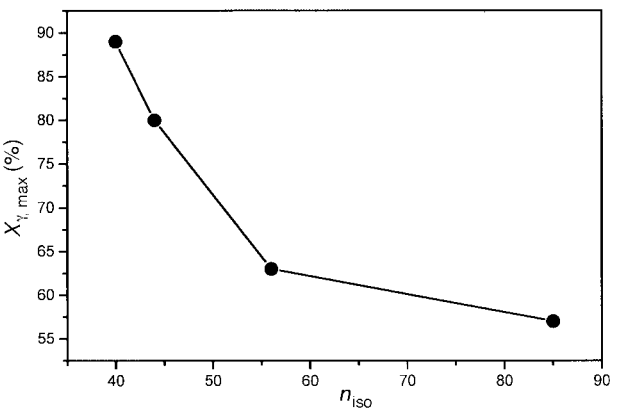

Fig. 7 Maximum content of the γ-modification of isotactic poly(propene) as a function of the isotactic segment length n_{iso}. The maximum γ-content was achieved at: $T_c=130$ °C for $n_{iso}=40$, $T_c=125$ °C for $n_{iso}=44$, $T_c=125$ °C for $n_{iso}=56$ and $T_c=132$ °C for $n_{iso}=85$.

ual metallocene catalysts. Since the formation of large spherulite types is prevented in favor of well defined superstructures smaller than the wavelength of visible light, the resulting poly(propene)s exhibit much better optical clarity and very low haze. Moreover, it should be very interesting to evaluate the performance of nucleating agents with respect to the predominant formation of either the α or γ modification of crystalline isotactic poly(propene).

Crystallization behavior of short-chain branched poly(ethene)s

In addition to steric irregularities introduced *via* regio- and stereo-irregularities occurring during propene polymerization, steric irregularities can result from random placement of short chain branches along the poly(alk-1-ene) backbone, thus interrupting crystallizable sequences. Two strategies lead to short-chain branched poly(ethene)s: (i) copolymerization of ethene with alk-1-enes such as oct-1-ene, using 'single-site' metallocene-based catalysts, and (ii) migratory insertion polymerization, producing methyl- and alkyl-branched poly(ethene)s by simultaneous insertion and migration of the transition metal alkyls. In the past, conventional multisite catalysts failed to produce ethene copolymers over the entire feasible composition range. Catalysts, developed for production of LLDPE with low alk-1-ene content (<5 mass%), gave low molecular mass wax-like fractions in a mixture with homopoly(ethene)s and ethene copolymers when the concentration of alk-1-enes was raised. Vanadium-based catalysts developed for production of ethene/propene/diene (EPDM) rubber failed to polymerize propene. With modern catalyst generations, *e.g.*, catalyst based upon MBI, excellent control of comonomer incorporation over the entire composition range is achieved, including homopoly(ethene) as well as isotactic homopoly(propene). The response of copolymerization efficiency to metallocene structure is displayed in Fig. 8, using copolymerization parameters r for ranking. Copolymerization parameters are defined as the ratio of the rate constants for homopropagation (k_{PP} or k_{EE}) with respect to those of heteropropagation (k_{PE} or k_{EP}). A set of two parameters is sufficient to describe copolymer architecture in a first order Markovian model: $r_E = k_{EE}/k_{EP}$, and $r_O = k_{OO}/k_{OE}$ for ethene copolymerization with oct-1-ene. The copolymerization parameters can be determined using the ^{13}C NMR spectroscopic sequence analysis of the copolymer.

It is very well recognized and apparent from Fig. 8 that bridged metallocene catalysts, *e.g.*, the syndioselective $Me_2C(Cp)(Flu)ZrCl_2$ or the isoselective $Me_2Si(2\text{-}Me\text{-}Benz\text{-}Ind)_2ZrCl_2$/MAO give much higher incorporation with respect to the conventional non-bridged metallocenes. Among bridged metallocenes, half-sandwich metallocenes such as $Me_2Si(CpMe_4)(NBu^t)TiCl_2$/MAO, referred to by Dow Chemical as 'constrained geometry' catalysts (abbreviated as CGC in Fig. 8), give highest comonomer incorporation. When using oct-1-ene content of 75 mol% in the monomer feed, 44 mol% oct-1-ene is incorporated in the poly(ethene-*co*-oct-1-ene) when polymerization is carried out in toluene at 40 °C. Even at high comonomer content, narrow molecular mass distributions typical for single-site metallocenes were observed. The performance of bridged and non-bridged metallocenes in ethene/alk-1-ene copolymerization was compared by Fink and co-workers[44,45] and Uozumi and Soga.[46] Within the metallocene family containing the silylene-bridged bisindenyl-ligand framework, Schneider and Mülhaupt[47] demonstrated that benzannelation promoted catalyst activity and oct-1-ene incorporation, whereas 2-methyl substitution gave much higher molecular mass of the copolymer but did not affect comonomer incoporation. The effect of benzannelation was confirmed by molecular modeling. In contrast to conventional catalyst systems, it is possible to prepare also stereoregular copolymers such as syndiotactic propene/alk-1-ene copolymers. The opportunity of controlling crystallization of syndiotactic poly(propene-*co*-oct-1-ene) was demonstrated by Thomann *et al.*[48]

Similar to the formation of regioirregularities (*cf.* Fig. 3), β-hydride transfer combined with rotation and '2–1'-type insertion can account for the formation of methyl branches during ethene polymerization. Moreover, as previously reported by Fink *et al.*,[19–21] especially group VIII transition metal alkyls with bulky ligands can migrate along the polymer chain by repeated β-hydride transfer and reinsertion of the transition metal hydride. When insertion takes place exclusively at the chain ends, methyl branched or linear poly(ethene)s are formed. As displayed in Fig. 9 insertion of transition metal alkyls, located somewhere in the polymer chain, gives short alkyl- and branched alkyl-side chains. This rather unusual behavior was observed by Brookhart and others[22] when he introduced bisimine-coordinated nickel and palladium catalysts which are activated with MAO or boranes to form cationic transition metal alkyl bonds as catalytically active intermediates.

Using either alk-1-ene comonomers or applying migratory insertion polymerization produces poly(ethene) chains interrupted by short-chain branching. The degree of branching, calculated as the number of branching carbon atoms per 1000 carbon atoms, can be varied either by varying the content of oct-1-ene incorporation in MBI/MAO-initiated ethene/oct-1-ene copolymerization, or by varying the polymerization conditions during migratory insertion. MBI/MAO catalyzed polymerization was reported in detail.[27,28,47,49] The migratory insertion homopolymerization was performed at 20, 40 and 60 °C in toluene, using the MAO-activated nickel complexes with dimethyl- (DMN) and non-substituted (DHN) bisimine ligand frameworks shown in Fig. 10, typically using Al/Ni molar ratios of 1000 mol $(mol)^{-1}$. The results of nickel-catalyzed polymerization as a function of polymerization conditions are listed in Table 1.

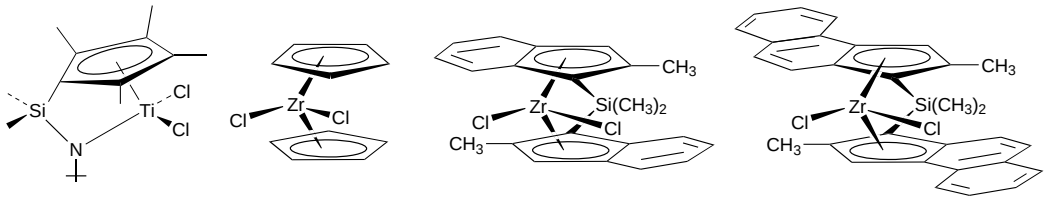

CGC	CP	MI	MBI
$r_O = 0.290$	$r_O = 0.05$	$r_O = 0.013$	$r_O = 0.118$
$r_E = 4.1$	$r_E = 32.8$	$r_E = 19.5$	$r_E = 10.1$
$r_e \cdot r_O = 1.19$	$r_e \cdot r_O = 0.17$	$r_e \cdot r_O = 0.25$	$r_e \cdot r_O = 1.20$

Fig. 8 Comparison of various metallocenes in ethene/oct-1-ene copolymerization [CGC = dimethylsilenyl(tetramethylcyclopentadienyl)-(*N*-*tert*-butylamido)titanium(IV) dichloride, CP = zirconocene dichloride, MI = *rac*-dimethylsilenylbis(2-methylindenyl)zirconium dichloride), MBI = *rac*-dimethylsilenylbis(2-methylbenz[e]indenyl)zirconium dichloride]

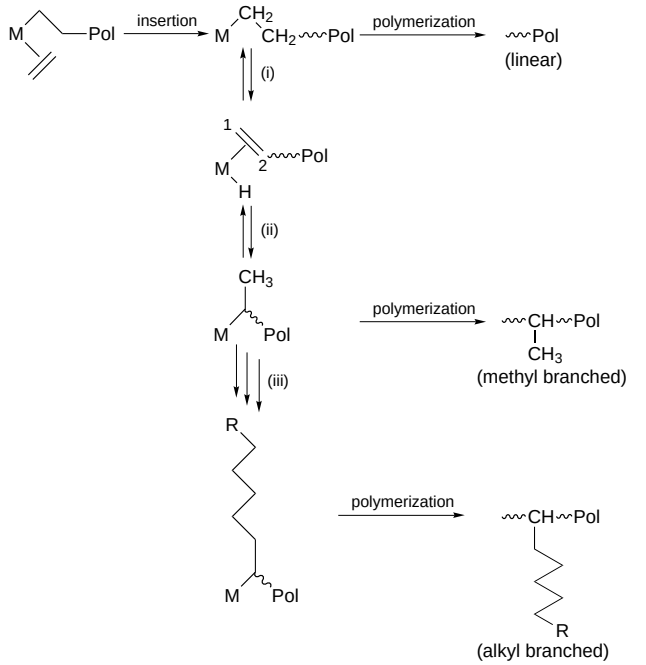

Fig. 9 Migratory insertion polymerization of ethene to produce branched poly(ethene)s. (i) β-H elimination and vinylidene-type endgroup, (ii) reinsertion of vinylidene-type endgroup, (iii) two or more subsequent β-H eliminations and reinsertions of vinylidene-type endgroups leading to alkyl branches

In accord with earlier observations by Brookhart, the melting temperature and the degree of branching, which is found to be preferred methyl-branching in the case of nickel bisimine catalysts, change with pressure and temperature as well as with substitution pattern of the bisimine ligand. At high polymerization temperatures, low ethene pressure and methyl substitution of the catalyst, branching of the poly(ethene) is favored. The correlation of poly(ethene) melting temperature with ethene concentration is plotted for polymerization using DMN and DHN and comparing DMN polymerization at different temperatures in Fig. 11. In contrast to corresponding Pd bisimine catalyst, all poly(ethene)s were semicrystalline with melting temperatures varying from 40 to 130 °C. According to ^{13}C NMR studies, methyl branching appears to be preferred over the entire composition range. The lowest melting temperatures were found for the poly(ethene) prepared by DMN/MAO catalysts at elevated polymerization temperatures.

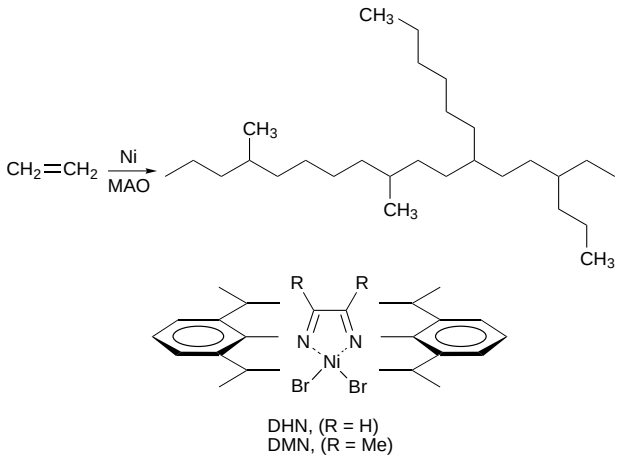

Fig. 10 Nickel catalysts used for migratory ethene homopolymerization

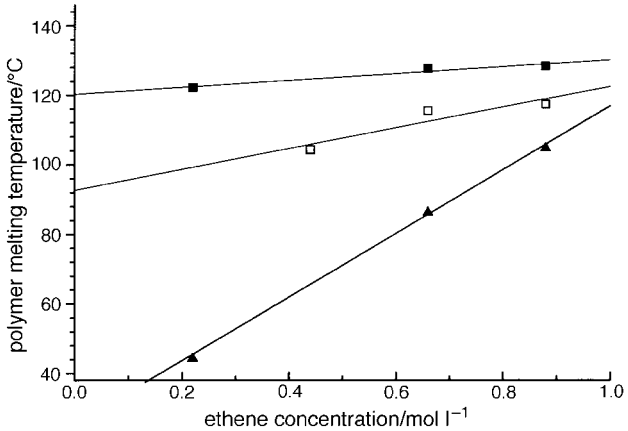

Fig. 11 Poly(ethene) melting temperature as a function of ethene concentration, nickel ligand framework and polymerization temperature [■, 20 °C (DHN); □, 60 °C (DHN); ▲, 20 °C (DMN)]

Interestingly, there exists a linear correlation between the degree of branching, measured as the number of branching C per 1000 C, and melting temperature, measured by means of DSC (Fig. 12). The slight deviation of copolymers produced on nickel-based catalysts could result from the different nature of the short-chain branches (Fig. 13). Since also side chain C atoms are counted in the total number of C atoms, there should be a slight deviation when comparing the C_6 hexyl side

Table 1 Ethene polymerizations using MAO-activated Ni-based DHN and DMN catalysts as a function of ethene pressure and polymerization temperature

	catalyst[a]	pressure[b]/bar	$f_{[E]}$[c]/mol l^{-1}	T_P[d]/°C	A[e]/kg (mol$_{Ni}$ h mol l^{-1})$^{-1}$	T_m[f]/°C	N[g]
PE01	DHN	1.5	0.22	20	2700	122	8
PE02	DHN	4.6	0.66	20	2090	128	6
PE03	DHN	6.1	0.88	20	850	129	4
PE04	DHN	5.2	0.44	60	800	104	23
PE05	DHN	8.0	0.66	60	860	115	12
PE06	DHN	10.6	0.88	60	240	117	15
PE07	DHN	3.3	0.66	0	740	129	1.0
PE02	DHN	4.6	0.66	20	2090	128	6
PE08	DHN	6.2	0.66	40	2420	120	7.0
PE05	DHN	8.0	0.66	60	860	115	12
PE09	DMN	1.5	0.22	20	1500	44	54
PE10	DMN	4.6	0.66	20	3080	86	31
PE11	DMN	6.1	0.88	20	2180	105	11

[a]DHN = DAD(H,H)NiBr$_2$, DMN = DAD(Me,Me)NiBr$_2$, [Ni] = 20 μmol l^{-1}, [Al] = 20 mmol l^{-1}. [b]Pressure in the polymerization vessel. [c]Ethene concentration in toluene calculated according to ref. 50. [d]Polymerization temperature. [e]Activity, calculated from the mass of the polymer, catalyst concentration, monomer concentration and polymerization time. [f]Determined by DSC (heating rate 20 K min^{-1}). [g]Number of branching carbons per 1000 carbon atoms, determined by $^1H/^{13}C$ NMR spectroscopy.

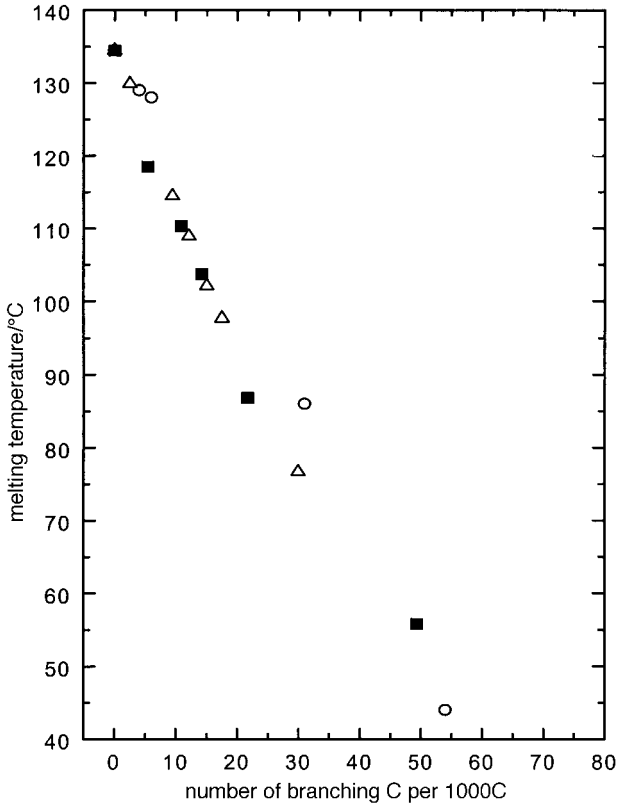

Fig. 12 Influence of the degree of branching of ethene/oct-1-ene copolymers, prepared with metallocene catalysts such as MBI and CGC and nickel catalysts displayed in Fig. 8 [△, GCG C_2/C_8 copolymer]; ■, MBI C_2/C_8 copolymer; O,Ni catalyst, branched poly(ethene)

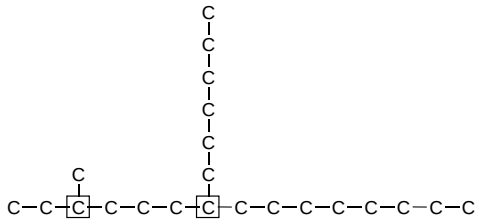

Fig. 13 Variation of the segment length of crystallizable poly(ethene) between two steric irregularities resulting from short chain branching

chain with respect to the short C_1 methyl side chain, especially at high oct-1-ene contents.

Crystallization behaviour of ethene/oct-1-ene

Fig. 14 shows WAXS traces of EO02, EO25, EO38 and EO55. The 110 and 200 reflections of poly(ethene) are indicated. The crystallinity decreases rapidly with increasing oct-1-ene content. The WAXS trace of EO25 shows weak reflections. EO38 and EO55 appear virtually amorphous and have a typical amorphous halo in the WAXS traces only.

Comparable results are obtained by PVT measurements. Fig. 15 shows the specific volume of the respective polymers as a function of temperature at ambient pressure. The specific volume of EO02 increases drastically at its melting point of *ca.* 130 °C. The change in v_{sp} is typical for first order phase transition. EO25 and EO38 show only small changes of the specific volume and broader melting regions, from ambient temperature to *ca.* 75 and 60 °C, respectively. This reflects a lowering of the melting temperature with increasing amount of oct-1-ene and simultaneously a decrease of the degree of crystallinity. In contrast to the WAXS measurements only EO55 is not crystalline.

AFM is able to provide detailed information on crystalline

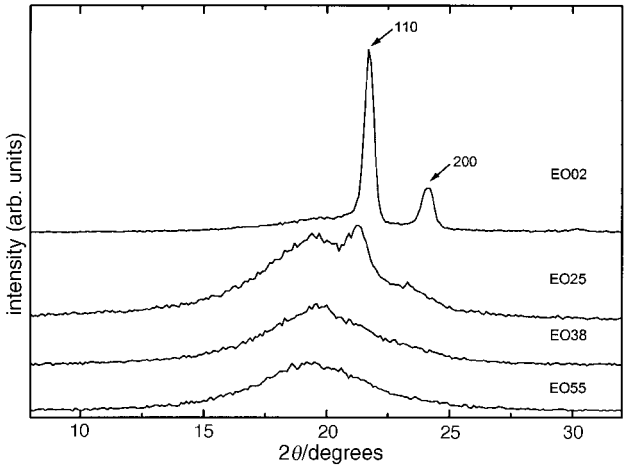

Fig. 14 WAXS traces of EO02, EO25, EO38 and EO55 (numbers refer to oct-1-ene incorporation in mass% of oct-1-ene). The 110 and 200 reflections are assigned according to neat poly(ethene).

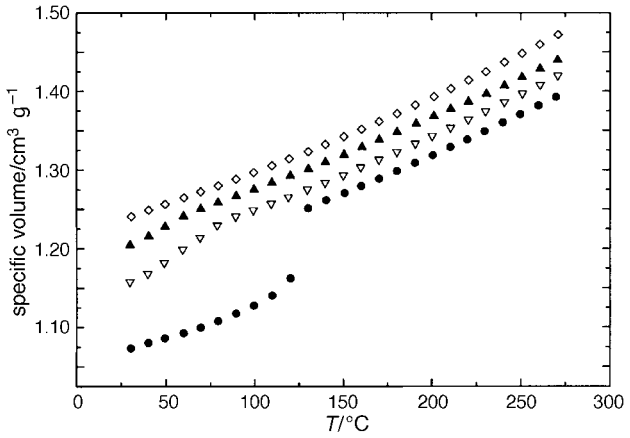

Fig. 15 Specific volume of EO02, EO25, EO38 and EO55 as a function of temperature at ambient pressure obtained by PVT measurements. The data points of EO25, EO38 and EO55 are shifted by the values given in brackets [◇, EO55 (+0.06); ▲, EO38 (+0.04); ▽, EO25 (+0.01); ●, EO02].

morphologies. Fig. 16(*a*)–(*e*) show AFM phase images of EO02, EO25, EO38 and EO55 that are cooled from the melt to room temperature with a cooling rate of 0.2 °C min^{-1}. Crystalline structures appear bright, amorphous regions dark. Fig. 16(*a*) shows the micrograph of EO02. The crystalline morphology is built up by broad lamellae. Fig. 16(*b*) depicts an AFM phase imaging of EO25 with low magnification. A branched morphology is visible, built up by irregular lamellae and crystalline grains. Fig. 16(*c*) shows an enlarged micrograph of the grain morphology. The grains typically have a diameter of 30 nm. Fig. 16(*d*) shows the crystalline morphology of EO38. Again grains are visible. These grains appear either singular or joined together in strings. The strings of grains have a length of *ca.* 100 nm. The diameter of the grains varies from 5 to 20 nm. Fig. 16(*e*) shows an AFM micrograph of EO55. The sample is completely amorphous. The white dots are typical artefacts.

The observed morphologies are consistent with a model given by Minick *et al.*[51] The model describes the change from a high crystalline, lamellar morphology to the granular morphology of low crystallinity copolymers. Fig. 17 shows a schematic illustration of the four types of crystalline morphologies:[51] type *a*: a well developed lamellar morphology, type *b*: less ordered lamellae, type *c*: bundle like crystals (also named fringed micella) that are able to form supermolecular structures like spherulites, type *d*: bundle like crystals that are unable to form supermolecular structures. Using this nomenclature the

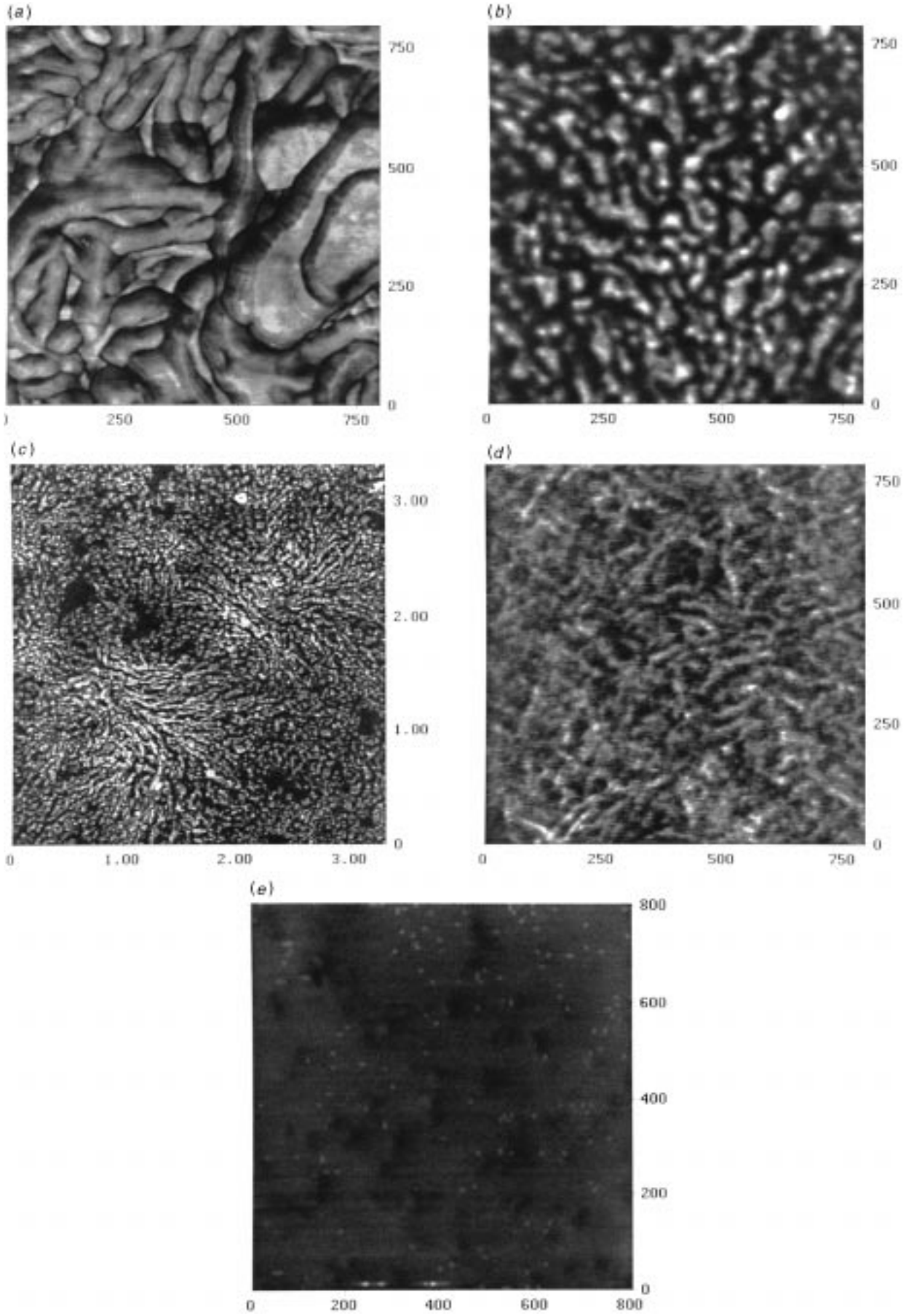

Fig. 16 AFM phase mode micrographs of etched samples: (*a*) EO02; (*b*) EO25; (*c*) as (*b*) enlarged; (*d*) EO38; (*e*) EO55

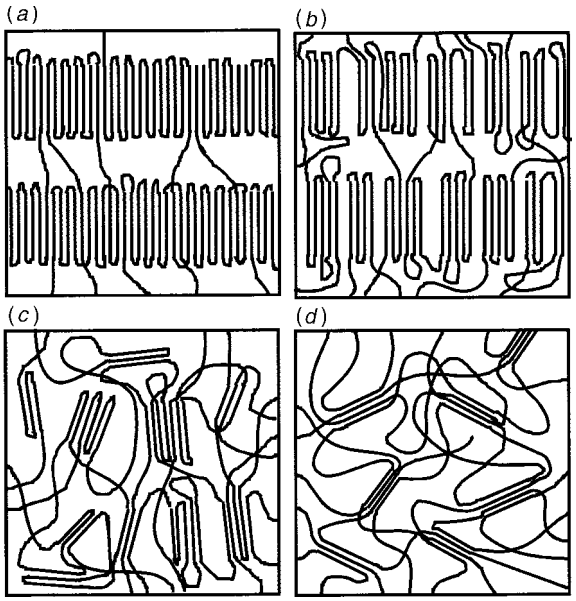

Fig. 17 Schematic illustration of the four types of crystalline morphologies as described by Minick *et al.*[50]

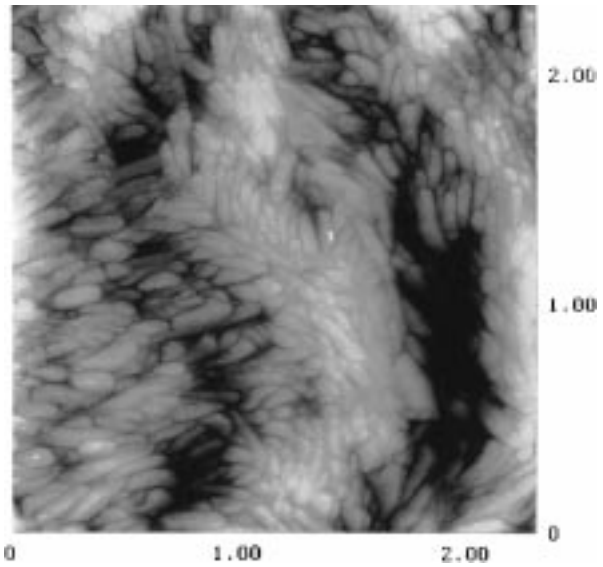

Fig. 18 AFM micrograph of the crystalline morphology of PE6. Well formed, short lamellae.

morphology found for EO02 can be classed as type *a* to type *b*, the morphology of EO25 as type *c* and the morphology of EO38 as type *d*.

A transition stage between lamellar and granular morphology is shown in Fig. 18. The AFM micrograph of polymer sample PE06 (*cf.* Table 1) was received after cooling the sample from the melt to room temperature at a cooling rate of 0.2 °C min^{-1}. The sample shows well formed lamellae. In contrast to the elongated lamella formed by neat poly(ethene) these lamellae are extremely short. It could be assumed that the ordered lamellar structure is disrupted by the introduction of defects. A further increase of the number of defects might lead to the formation of granular morpholgies.

Conclusions

Metallocene-catalyzed alkene homo- and co-polymerization as well as migratory insertion polymerization give excellent control of molecular architectures of poly(alkene)s and allow one to place random steric irregularities into the poly(alkene) backbone. This synthetic route to poly(alkene)s with modified molecular architectures represents the key to controlled polymer crystallization. Owing to the very uniform nature of novel homo- and co-polymers, novel poly(alk-1-ene)s can be applied to study the basic correlations between catalyst structure, polymer architecture, and polymer properties. This will be of special interest for the development of novel poly(alk-1-ene) materials, which exhibit improved processing properties and give much better control of morphology development and toughness/stiffness balance. Manipulation of catalyst ligand structure represents a very promising route to controlled poly(alk-1-ene) molecular and supermolecular architectures, which represent fingerprints of the catalyst systems.

The authors would like to thank the Bundesminster für Bildung und Forschung for supporting our research on metallocene-catalyzed alkene copolymerization (project no. 03M40719) and on controlled copolymerization of functionalized alk-1-enes (project no. 03N1028 0).

References

1 *Polypropylene Handbook*, ed. E. P. Moore, jr., Hanser Publishers, Munich, 1997.
2 H. H. Brintzinger, D. Fischer, R. Mülhaupt, B. Rieger and R. M. Waymouth, *Angew. Chem., Int. Ed. Engl.,* 1995, **34**, 1143.
3 W. Kaminsky, *Macromol. Chem. Phys.*, 1996, **197**, 3907.
4 A. E. Hamiliec and J. B. P. Soares, *Prog. Polym. Sci.,* 1996, **21**, 651.
5 J. A. Ewen, R. L. Jones, A. Razavi and J. D. Ferra, *J. Am. Chem. Soc.*, 1988, **110**, 339.
6 B. Lotz, J. C. Wittmann and A. J. Lovinger, *Polymer,* 1996, **37**, 4979.
7 G. H. Llinas, S. H. Dong, D. T. Mallin, M. D. Rausch, Y. G. Lin, H. H. Winter and J. C. W. Chien, *Macromolecules*, 1992, **25**, 1292.
8 G. W. Coates and R. M. Waymouth, *Science*, 1995, **267**, 217.
9 J. C. W. Chien, Y. Iwamoto, M. D. Rausch, W. Wedler and H. H. Winter, *Macromolecules*, 1997, **30**, 3447.
10 L. Resconi, R. L. Jones, A. L. Rheingold and G. P. A. Yap, *Organometallics,* 1996, **15**, 998.
11 L. Resconi and R. Silvestri, *in Polymeric Materials Encyclopedia*, ed. J. C. Salamone, CRC Press, Boca Raton, FL, 1996, vol. 9, p. 6609.
12 Y. W. Cheung and M. J. Guest, *ANTEC*, 1996, **96**, 1643.
13 F. G. Sernetz, R. Mülhaupt, F. Amor, T. Eberle and J. Okuda, *J. Polym. Sci. Part A: Polym. Chem.,* 1997, **35**, 1571.
14 C. Pellecchia, D. Pappalardo, M. Darco and A. Zambelli, *Macromolecules*, 1996, **29**, 1158.
15 A. Batistini, *Macromol. Symp., 1995,* **100**, 137.
16 H. Cherdron, M.-J. Brekner and F. Osan, *Angew. Makromol. Chem.*, 1994, **223**, 121.
17 G. M. Bendekit, B. L. Goodall, M. S. Marchant and L. F. Rhodes, *New J. Chem.*, 1994, **18**, 105.
18 F. G. Sernetz, R. Mülhaupt and R. M. Waymouth, *Polym. Bull.*, 1997, **38**, 141.
19 G. Fink, V. Möhring, A. Heinrichs, C. Denger, R. H. Schubbe and P. H. Mühlenbrock, *in Polymeric Materials Encyclopedia*, ed. J. C. Salamone, CRC Press, Boca Raton, FL, 1996, vol. 6, p. 4720.
20 G. Fink, V. Möhring, A. Heinrichs and Ch. Denger, *ACS Symp. Ser.*, 1992, **496**, 88.
21 R. Schubbe, K. Angermund, G. Fink and R. Goddard, *Macromol. Chem. Phys.*, 1995, **196**, 467.
22 (*a*) G. van Koten and K. Vrieze, *Adv. Organomet. Chem.*, 1982, **21**, 151; (*b*) L. K. Johnson, C. M. Killian and M. Brookhart, *J. Am. Chem. Soc.*, 1995, **117**, 6414.
23 L. K. Johnson, S. Mecking and M. Brookhart, *J. Am. Chem. Soc.*, 1996, **118**, 267.
24 D. Fischer and R. Mülhaupt, *J. Organomet. Chem.*, 1991, **417**, C7.
25 U. Stehling, J. Diebold, R. Kirsten, W. Röll, H. H. Brintzinger, S. Jüngling, R. Mülhaupt and F. Langhauser, *Organometallics*, 1994, **13**, 964.
26 M. J. Schneider and R. Mülhaupt, *J. Mol. Catal Part A: Chemical*, 1995, **101**, 11.
27 J. Suhm, M. J. Schneider and R. Mülhaupt, *J. Polym. Sci. Part A*, 1997, **35**, 735.
28 J. Suhm, R. D. Maier, J. Kressler and R. Mülhaupt, *Acta Polym.*, in preparation.
29 P. Zoller, P. Bolli, V. Pahud and H. Ackermann, *Rev. Sci. Instrum.*, 1976, **49**, 948.
30 J. C. Randall, *Macromolecules*, 1997, **30**, 803.

31 Y. Vanderleck, K. Angermund, M. Reffke, R. Kleinschmidt, R. Goretzki and G. Fink, *Eur. J. Chem.*, 1997, **3**, 585.
32 S. Jüngling, R. Mülhaupt, U. Stehling, H. H. Brintzinger, D. Fischer and F. Langhauser, *J. Polym. Sci., Part A: Polym. Chem.*, 1995, **33**, 1305.
33 A. Grassi, A. Zambelli, L. Resconi, E. Albizzati and R. Mazzochi, *Macromolecules*, 1988, **21**, 617.
34 B. Rieger and J. C. W. Chien, *Polym. Bull.*, 1989, **21**, 159.
35 D. Fischer and R. Mülhaupt, *Macromol. Chem. Phys.*, 1994, **195**, 1433.
36 S. Jüngling, Dissertation, Universität Freiburg, 1995.
37 W. Spaleck, M. Antberg, M. Aulbach, B. Bachmann, V. Dolle, S. Haftka, F. Küber, J. Rohrmann and A. Winter, *in Ziegler Catalysts*, ed. G. Fink, R. Mülhaupt and H. H. Brintzinger, Springer Publ., Berlin, 1995, p. 83.
38 G. Natta and P. Corradini, *Nuovo Cimento Suppl.*, 1960, **15**, 40.
39 B. Lotz, S. Kopp and D. Dorset, *C. R. Acad. Sci. Paris*, 1994, **319**, *Ser. IIb*, 187.
40 S. V. Meille, S. Brückner and W. Porzio, *Macromolecules*, 1990, **23**, 4114.
41 B. Lotz and J. C. Wittmann, *J. Polym. Sci., Polym. Phys.*, 1986, **24**, 1541.
42 D. C. Bassett and R. H. Olley, *Polymer*, 1984, **25**, 935.
43 R. Thomann, Ch. Wang, J. Kressler and R. Mülhaupt, *Macromolecules*, 1996, **29**, 8425.
44 P. Mühlenbrock and G. Fink, *Z. Naturforsch. Sect. B-A, J. Chem. Sci.*, 1995, **50**, 423.
45 J. Koivumaki, G. Fink and J. V. Seppälä, *Macromolecules*, 1994, **27**, 6254.
46 T. Uozumi and K. Soga, *Makromol. Chem.*, 1992, **193**, 823.
47 M. J. Schneider, J. Suhm, R. Mülhaupt, M. H. Prosenc and H. H. Brintzinger, *Macromolecules,* 1997, **30**, 3164.
48 R. Thomann, J. Kressler and R. Mülhaupt, *Macromol. Chem. Phys.*, 1997, **198**, 1271.
49 M. J. Schneider and R. Mülhaupt, *Macromol. Chem. Phys.*, 1997, **198**, 1121.
50 W. Krauss and W. Gestrich, *CHEMTECH.*, 1977, **6**, 513.
51 J. Minick, A. Moet, A. Hiltner, E. Baer and S. P. Chum, *J. Appl. Polym. Sci.*, 1995, **58**, 1371.

Paper 7/06451I; *Received* 3*rd September*, 1997